Evolution of Baryon Rich Quark-Gluon Plasma and radiation of Single Photons

S. V. S. Sastry, D. Dutta, A. K. Mohanty and D. K. Srivastava*
Nuclear Physics Division, Bhabha Atomic Research Centre, Trombay, Mumbai 400 085, India
* VECC, 1/AF Bidhan Nagar, Kolkata 700 064, India
* Duke University, Dept. of Physics, Box 90305, Durham, NC 27708-0305.

Abstract

The (3+1) dimensional expansion of the quark gluon plasma (QGP) produced at finite baryon density has been studied using relativistic hydrodynamical approach. The pressure functional of the equation of state (EoS) has been determined for the interacting nuclear matter with mesons exchange. The EoS has been used to solve hydrodynamical equations using RHLLE algorithm. The space time expansion of the plasma has been studied for the cases of SPS energy and RHIC energy both at finite baryon density and for a hypothetical case of SPS energy at zero baryon density. The space-time evolution is slowed and the life times of QGP and mixed phases are shortened in the presence of finite baryon density. The space time integrated total photon yields have been estimated by convoluting the static emission rates with the space time expansion of the plasma. It has been shown that the total photon yield at zero rapidity is not significantly affected by the baryon density for SPS energy. The total photon yield is unaffected by the Landau-Pomeranchuk-Migdal effect at SPS energy at zero baryon density, as the quark matter contribution to photon yield is less compared to hadronic matter.

Electromagnetic processes such as photons and dileptons production are important to identify the quark gluon plasma (QGP) expected to be formed in the ultra relativistic heavy ion collisions at SPS, RHIC and LHC energies [1, 2, 3, 4]. Consequent to the availability of the experimental data reported by WA98 collaboration [5] of single photons from Pb+Pb collisions at CERN SPS, these studies gained much interest in recent times. The experimental spectra however include photons coming from various sources like decays, prompt and thermal photons. Photons are produced at each stage from an expanding volume of plasma being both in QGP and hadron phases. The yields of these electromagnetic signals are quite sensitive to the space time evolution of the QGP. Assuming a first order phase transition, the plasma will expand and evolve through a QGP, mixed and hadron phases governed by the appropriate equation of state. Thermal photons are emitted at a later stage which depends on the space time evolution scenario considered consequently, the expansion dynamics determines the observed spectra. Initially, the plasma expands longitudinally, however at high energy densities and when plasma life time is large, the transverse expansion effects become significant and can not be ignored [6]. Further, the experimental data indicates the presence of finite baryon density at freezeout temperature. The evolution becomes more complicated if the plasma is unsaturated or formed at finite baryon density. These physical conditions of the plasma affect both the basic photon production rate and also the total space time integrated photon yields. In the present work we incorporate the finite baryon density effects in both the production rates and the plasma expansion dynamics.

The photon production rates from QGP phase have been investigated in detail in [7]-[17]. These studies include the production rates at effective one loop and two loop levels. Further, multiple soft scatterings of the fermion during photon emission reduce the photon coherence lengths, known as Landau-Pomeranchuk-Migdal (LPM) effect, and suppress the production rates [12,

15, 16]. The photon rates from the hadron phase were estimated considering the comprehensive set of processes in [7, 18], and the prompt decays were estimated in [19, 20]. Several groups have already reported the space-time integrated photon yield calculations for SPS, RHIC and LHC energies considering (i) various sets of equations of state, (ii) considering one or three dimensional space time expansion of plasma, (iii) with or without boost invariance, for details see [1, 2, 3, 4, 6, 21, 22].

In the following, the expansion dynamics of the plasma is determined by the EoS and the relativistic hydrodynamical equations. The conservation equations for the energy (E), momentum (M) and net baryon number (R) densities are given by,

$$\partial_\mu T^{\mu\nu} = 0 \quad \text{and,} \quad \partial_\mu N^\mu = 0 \tag{1}$$

$$E = T^{00} = (\epsilon + p)\gamma^2 - p \tag{2}$$

$$\mathbf{M} = T^{0i} = (\epsilon + p)\gamma^2 \mathbf{v} \tag{3}$$

$$R = N^0 = nu^0 = n\gamma \tag{4}$$

Here, $u^\mu = \gamma(1, \mathbf{v})$ is the fluid velocity. In the above, ϵ, p, n are the energy, pressure and net baryon number densities in the local rest frame of the fluid. The conservation equations for E, M, R of Eqs. (2-4) for cylindrical geometry with the longitudinal (z-axis) boost invariance and at z=0 are as discussed in [23]. The shock just at the QGP formation time is represented by the Riemann initial value problem. The full solution to the Riemann problem is approximated by the Godunov scheme consisting of a rarefaction wave and the contact discontinuity. This scheme approximates the Riemann shock propagation by assuming a region of constant flow between the discontinuous surfaces. Our present calculations have been performed using Relativistic HLLE (RHLLE) program to solve the hydrodynamical equations [23, 24]. An important input for this method is the equation of state (EoS) specifying the pressure as a functional of the energy density and the number density $p(\epsilon, n)$. Once an EoS is specified, the hydrodynamical equations uniquely determine the expansion dynamics. We obtain the EoS for hadronic, mixed and QGP states at finite baryon density. In this study, the EoS for the QGP state is taken from bag model consisting of u,d quarks and gluons. The pressure, energy and entropy densities are given by,

$$p = \frac{37\pi^2}{90}T^4 + \frac{1}{9}(\mu T)^2 + \frac{1}{162\pi^2}\mu^4 - B \tag{5}$$

$$p = (\epsilon - 4B)/3 \ ; \ s = \frac{\partial P}{\partial T}|_\mu \ ; \ \epsilon = Ts + \mu n - p \tag{6}$$

In above, the μ is the baryo chemical potential representing the finite baryon density effects. The hadronic EoS is obtained from a general class of thermodynamically self consistent equations of the interacting nuclear matter that reproduce the ground state matter properties. The present EoS includes the σ, ω mesons interacting with nucleons and anti nucleons (i.e. masses upto 1.0 GeV) and a free gas of π, ρ, η mesons. The hadron pressure (p_h), net baryon number density (n), the scalar density (ρ) and the partial pressures of baryon and mesons (p_N, p_i) are as in [25] given by,

$$p_h(T, \mu) = p_N + \Sigma_i p_i + n\nu(n) - \int_0^n \nu(n')dn' - \rho_s \mathbf{S}(\rho_s) + \int_0^{\rho_s} \mathbf{S}(\rho_s')d\rho_s' \tag{7}$$

$$n(T, \mu) = \frac{g_N}{(2\pi^3)} \int d^3k \left[f_T(E_k^*, \nu) - f_T(E_k^*, -\nu) \right], \quad \text{with} \quad \nu = \mu - \nu(n) \tag{8}$$

$$\rho(T,\mu) = \frac{g_N}{(2\pi^3)} \int d^3k \frac{M^*}{E_k^*} \left[f_T(E_k^*, \nu) + f_T(E_k^*, -\nu) \right] \tag{9}$$

$$E_k^* = \sqrt{k^2 + M^{*2}} \; ; \quad M^* = M - \mathbf{S}(\rho_s) \quad ; \quad \nu(n) = C_v^2 n - C_d^2 \rho_s \; ; \; \mathbf{S}(\rho_s) = C_s^2 \rho_s \tag{10}$$

$$p_N = T \frac{g_N}{(2\pi^3)} \int d^3k \left[\ln(1 + e^{-(E_k^* - \nu)/T}) + \ln(1 + e^{-(E_k^* + \nu)/T} \right] \tag{11}$$

$$p_i(T; m_i) = -T \frac{g_i}{(2\pi^3)} \int d^3q \left[\ln(1 - e^{-(\sqrt{q^2 + m_i^2}/T)}) \right] \tag{12}$$

In the above, f_T is the fermi distribution at temperature T and baryo chemical potential μ representing the baryon density. m_i are the meson masses, M is the nucleon bare mass and g_i, g_N are the meson and nucleon spin-isospin degeneracies. The energy density (ϵ) and entropy (s) are obtained using thermodynamic relations as in Eq. 6. The effective chemical potential $\nu(n)$ and the effective mass M^* are obtained using the parameters given in $C_v^2 = 238.08 GeV^{-2}$, $C_s^2 = 296.05 GeV^{-2}$, $C_d^2 = 0.183$ [25]. The Eqs.(8,9,10) are solved self consistently . The phase boundary in T, μ plane, shown in Fig. 1(a), is obtained from the Gibbs conditions given by,

$$p_h = p_q, \qquad T_h = T_q, \qquad \mu_h = \mu_q \tag{13}$$

The mixed phase for a given (ϵ,n) is obtained from,

$$\epsilon = \lambda_q \epsilon_q(T^*) + (1 - \lambda_q)\epsilon_h(T^*) \qquad \text{and} \qquad n = \lambda_q n_q(T^*) + (1 - \lambda_q) n_h(T^*) \tag{14}$$

In the above, the subscripts μ, h denote the qgp,hadron phases. λ_q is the fraction of volume occupied by the QGP in the mixed phase. The EoS specifies the pressure as a functional of p(ϵ,n) in the required region in (ϵ,n) plane as shown in the Fig. 1 (nearly same as Fig. 1 of [25]). Fig. 1(a) shows the transition temperature and chemical potential given by Eq. 13. The transition temperature at zero baryon density is 169.9 MeV. Fig. 1(b) shows the energy density variation and the Fig. 1(c) shows the number density variation along the curve of Fig. 1(a). Fig.1(d) shows the energy density and number density for both quark and hadron phases for T, μ values along the curve of Fig. 1(a). The hadron phase is the narrow strip in the semi-infinite (ϵ,n) plane as shown in Fig. 1(d) by the mixed phase above and below by the $T = 0$ line of hadron phase. However, owing to small life times of QGP and mixed phases (10-20 fm/c), these phases occupy very small region of space time evolution diagrams which will be discussed later (Fig. 2). The T^* of Eq. 14 are determined using Figs. 1(b,c,a). The constants used in Fig. 1 are $\epsilon_0 = 0.1477 \hbar^3 GeV^4$ and $n_0 = 0.16 \hbar^3 GeV^3$.

We studied the expansion dynamics at finite baryon density for two cases; case (i) for SPS energy and case (ii) for the RHIC energy. The case (iii) for SPS energy at zero baryon density is studied to compare the effects of finite baryon density. The initial energy density and the number density at time $\tau = \tau_i$ have been assumed to be of wounded nucleon form, as given by $f(r) = \frac{3}{2}\sqrt{1 - \frac{r^2}{R^2}}$ and R is the nuclear radius taken to be 6.0 fm. The formation times are taken as τ_i=1 fm/c for SPS energy and τ_i=0.6 fm/c for the RHIC energies respectively. The parameters for RHIC energies were taken from [23]. The entropy (s), energy and number densities corresponding to SPS case of 158 AGeV of Pb+Pb collision is obtained by solving the simultaneous equations given by,

$$\pi R^2 n_b \tau_i = \frac{dN_B}{dy}$$

$$\pi R^2 s \tau_i = 3.6 \frac{dN}{dy}$$

We have taken $\frac{dN_B}{dy} = 80$, and $\frac{dN}{dy} = 700$ from the experimental data, which corresponds to a baryon density of n_b/n_0=4.5 . These space-time evolution of the plasma for the cases of SPS energy at finite baryon density is shown in Fig. 2 for different phases as indicated in the figure in various colors. The evolution of zero baryon density is also shown in Fig. 2, by thick colored lines representing the boundary of corresponding phases. The radial extension and the proper time (at z=0) are in units of nuclear radius. The outermost envelope of the hadron phase in Fig. 2 corresponds to the freeze out isotherm taken to be 120.0 MeV. The QGP phase region is almost the same for the two cases (slightly less at finite density). It can be seen in Fig. 2 that at SPS energy the baryon density decreases the life times of QGP and mixed phases of the plasma as well as the freeze out time. The transverse extension is also affected by the baryon density. Similar cases of space time evolution have been studied for RHIC energy. At RHIC energies, the life times are considerably larger together with the large transverse extension (see Fig.2 of [23]).

The temperature, chemical potential, constant energy density and the transverse velocity profiles in the space time, as the plasma expands, have been studied for these cases. The initial temperatures are larger in the QGP phase which in time go over to the constant temperature profiles corresponding to mixed phases. Subsequently, the temperature falls very rapidly as the plasma cools. The maximum temperatures (at r=0 for wounded nucleon form) reached are approximately 239.06 MeV, 244.25 MeV for SPS energies for the cases of with and without baryon density respectively and 348.4 MeV at RHIC energy. The average energy densities correspond to the temperatures of 214 MeV, 219.5 MeV at SPS energy for the cases of with and without baryon density. These results are comparable to those of Table 1 of [21].

The energy flow in space-time while in expansion is demonstrated by the constant energy contours. These contours for the SPS cases have been compared in Fig. 3. The solid curves are with baryon density and the dashed curves are for zero density. The constant energy density values are as mentioned in the figure in units if GeV/fm^3. It can be seen from the figures that the energy flow gets slower in the presence of baryon density. Similarly, the constant transverse velocity profiles for various values of $\beta = v/c$ have been shown for these cases in Fig. 4.

In the following we discuss the static rates for photon emission needed to calculate the total photon yields. The annihilation processes ($q\bar{q} \to g\gamma$) and the QCD Compton ($qg \to q\gamma$, $\bar{q}g \to \bar{q}\gamma$) processes have been considered for the thermal photon production at effective one loop level [7, 9]. The photon emission rates from quark matter at one loop have been taken from the Traxler *et al.* [9], and at two loop level for non zero chemical potentials as reported in [17]. We reported the photon production rate upto two loop level for a general case of chemically unsaturated plasma at finite baryon density in [17]. The bremsstrahlung and annihilation with scattering (**aws**) processes at two loop level have been considered. At finite baryon density, the photon production at one loop level is dominated by the compton process compared to annihilation process. At two loop level, the bremsstrahlung radiation is affected whereas the **aws** process is insensitive to the baryon density presence. The bremsstrahlung radiation from quark is enhanced and from anti quark is suppressed at finite baryo chemical potential.

The photon emission rates from the hadron phase is determined by considering various meson reactions, such as $\rho \to \pi\pi\gamma$, $\pi\rho \to \pi\gamma$, $\pi\pi \to \rho\gamma, \omega \to \pi\gamma$. The $\pi\rho \to \pi\gamma$ estimate also includes the a_1 intermediate resonance. The numerical results of a detailed study of these decays [7] has been fitted by analytical expressions as a function of temperature and photon energy, as reported in [26, 27, 1]. In the present work, we used these analytical formulae for the photon rate calculations. It has been shown that from temperature in the range of 100-200 MeV, these formulae reproduce quite well the numerical results from detailed calculations for the photon energies from 200 MeV and upto 5.0 GeV. The one dimensional expansion of the plasma with

boost invariance has been already studied with these emission rates with and without baryon density. It was found that the finite baryon density has no effect on the total photon yields [28]. The total photon yield integrated over the plasma space-time hyper volume at zero rapidity is given by,

$$\frac{dN}{d^2P_T dy} = \int_{\tau_i}^{\tau_f} \tau d\tau \int_0^{R_f} r dr \int_0^{2\pi} d\phi \int_{-\infty}^{\infty} d\eta \left(\frac{EdR}{d^3p}|_q + \left(\lambda \frac{EdR}{d^3p}|_q + (1-\lambda)\frac{EdR}{d^3p}|_h \right) + \frac{EdR}{d^3p}|_h \right) \tag{15}$$

In above, the subscripts q and h denote the photon emission rates from QGP and hadron phases. The τ_f and R_f denote the freeze out (outermost) boundary shown in Fig. 2. The rates correspond to the photons emitted in a fluid rest frame. In order to compare with the experimental photon yields, the transverse velocity distributions of Fig. 4 have been used to transform the photon energy as given by $E_\gamma = p^\mu u_\mu$. Fig. 5 shows the photon transverse momentum rapidity density distributions at zero rapidity for the 158 A GeV SPS energy for Pb+Pb collision compared with WA98 data. The finite and zero density cases are shown in figure. As seen in figure, the finite baryon density has very little effect on the photon spectrum, though the yield seems to be reduced marginally. This result is surprising considering that the expansion dynamics is affected as shown in Fig. 2. However, at these SPS energies, the overall plasma life time is small and the expansion effects and modified emission rates due to finite chemical potential cancel each other. However, the fit to experimental data is slightly improved when the finite density is considered (see Fig. 5). The prompt contribution in the present study has been taken from [19]. It has been noticed that the prompt estimates of [20] and [19] differ by about a factor of two together with roughly same slope in the region of 1.5-4 GeV. Therefore, if one considers the prompt contribution twice as large as given in [19], our calculated spectrum at finite density matches well with the experimental data. At RHIC energies, the baryon number densities are smaller and the finite density effects can be completely ignored. All these studies have been repeated for SPS case for different formation times τ_i=1.1 fm/c,1.2 fm/c and the results are very much similar. The results for photon yields have not changed significantly with different formation times studied. The present study was partly reported in [29].

The photon rates from QGP phase at two loop level of [17] are identical to the results of Aurenche *et al.* [11] for the equilibrated plasma, corrected by a factor of four. These rates and the total photon transverse momentum distributions shown in Fig. 5 for zero baryon density donot include the LPM effects. The effective two loop contributions to photon production rate from QGP phase consisting of bremsstrahlung and **aws** processes with and without LPM effect are discussed in [15, 16], especially as shown in Fig. 7 of Ref. [16]. We have studied the consequences of photon rate inhibition due to LPM effect on the space time integrated photon yields for the case of zero density. For this purpose, we used the phenomenological expressions of [16] that include LPM effects. The ratio of total photon yield arising from the two loop processes with and without LPM effect been estimated and shown in Fig. 6. It has been found that the LPM effect has not changed the photon transverse momentum distribution, due to the fact that at SPS energy the quark matter contribution to photon yield is very less. The LPM effect becomes important at higher energies as the **aws** contribution to photon emission is more suppressed. The total quark matter contribution from one and two loop processes without LPM effects are calculated and the relative percentage contribution of one loop processes and the two loop processes have been obtained for the space-time integrated yields. It should be noted that the temperature and the chemical potential dependence has been integrated out through the space time integrations of Eq. 15 over the plasma volume. These are also shown in Fig. 6 where short dashes represent oneloop/total quark matter emission and long dashes similarly for the two loop contribution. The different color curves show the results for RHIC energy. At RHIC

energies the LPM effects are important as the QM contribution is important and therefore the affects the calculated yields.

Conclusion

The effects of finite baryon density and the (3+1) dimensional expansion of the quark gluon plasma has been studied for SPS and RHIC energies. The transverse expansion has been obtained following relativistic hydrodynamical approach and the relativistic HLLE method. The equation of state for pressure functional has been obtained considering various mesons and interacting nucleons. The space time evolution of the QGP is shown to be affected by the baryon density. The radial and the temporal extension of the plasma is shorter in the presence of finite baryon density. The total plasma space time integrated photon yields have been compared for various cases in the presence of baryon density. Calculations at SPS energies with and without baryon density showed that the total photon yield is not very sensitive to the baryon density, however individual contributions to photon yields from various phases differ. The LPM effect is also found to be not affecting the photon yields for SPS energies, where as at RHIC energy this effect is important.

We acknowledge the fruitful discussions with Dr. S. Kailas.

References

[1] Thomas Peitzman and Markus H. Thoma, hep-ph/0111114.

[2] J. Alam, S. Raha and B. Sinha, Physics Reports **273** 243 (1996).

[3] D. K. Srivastava*et. al.,* Eur.Phys.J.**C12** 109 (2000); Erratum, nucl-th/0103014.

[4] D. K. Srivastava and B. Sinha, Phys. Rev. **C64** 034902 (2001) [nucl-th/0006018].

[5] M. M. Agarwal et al . WA98 Collaboration nucl-ex/0006007;, Phys. Rev. Lett. **85**, 3595 (2000)

[6] J. Alam, D. K. Srivastava, B. Sinha and D. N.Basu, Phys. Rev. **D48** 1117 (1993).

[7] J. Kapusta, Peter Lichard and David Seibert, Phys. Rev. **D44** 2774 (1991); Erratum *ibid.* **D47** 4171 (1993).

[8] R. Baier, H. Nakkagawa, A. Neigawa, K. Reidlich, Z. Phys. **C53** 433 (1992).

[9] C. T. Traxler and Markus H. Thoma Phys. Rev. **C53** 1348 (1996).

[10] C. T. Traxler, H. Vija and Markus H. Thoma Phys. Lett. **B346** 329 (1995).

[11] P. Aurenche, F. Gelis, R. Kobes and H. Zaraket, Phys. Rev. **D58** 085003 (1998), [hep-ph/9804224].

[12] P. Aurenche, F. Gelis, and H. Zaraket, Phys. Rev. **D61** 116001 (2000) [hep-ph/9911367] ; Phys. Rev. **D62** 096012 (2000) [hep-ph/0003326]

[13] P. Aurenche, F. Gelis, R. Kobes and E. Petitgirard, Phys. Rev. **D54** 5274 (1996) [hep-ph/9604398].

[14] P. Aurenche, hep-ph/0201011 ; Francois Gelis, hep-ph/0104067 ; Charles Gale, hep-ph/0104235.

[15] Peter Arnold, Guy D. Moore and Laurence G. Yaffe, hep-ph/0111107

[16] Peter Arnold, Guy D. Moore and Laurence G. Yaffe, hep-ph/0109064.

[17] D. Dutta, S. V. S. Sastry, A. K. Mohanty, K. Kumar and R. K. Choudhury, hep-ph/0104134 ; Submitted for publication.

[18] S. Sarkar, J. Alam, P. Roy, A. K. Dutt-Mazumder, B. Dutta-Roy and B. Sinha, Nucl. Phys **A634** 206 (1998); P. Roy *et al.* Nucl. Phys. **A653** 206 (1998).

[19] Cheuk-Yin wong and Hui Wang, Phys. Rev. **C58** 376 (1998).

[20] K. Gallmeister, B. Kempher and O. P. pavlenko, Phys. Rev. **C62** 057901 (2000) [hep-ph/000613] ; hep-ph/0009025.

[21] P. Huovinen, P. V. Ruuskannen, S. S. Rasanen, nucl-th/0111052.

[22] Jan-e Alam, nucl-th/0202021. ; Jan-e Alam, S. Sarkar, T. Hatsuda, Tapan K. Nayak and B. Sinha hep-ph/0008074.

[23] A. Dumitru and D. H. Rischke, nucl-th/9806003/v4.

[24] D. H. Rischke and M. Gyulassy, Nucl. Phys. **A608** 479 (1996).

[25] D. H. Rischke, Y. Pursun and J. A. Marhun, Nucl. Phys. **A595** 383 (1995).

[26] H. Nadeau, J. Kapusta and P. Lichard, Phys. Rev. **C45** (1992) 3034; **C47** 2426 (1993).

[27] F. D. Steffen and Markus H. Thoma, Phys. Lett.**B510** (2001) 1998 [hep-ph/0103044].

[28] D. Dutta, S. V. S. Sastry, A. K. Mohanty, K. Kumar and R. K. Choudhury, Presented in ICPA-QGP-'01, Nov 2001, held at Jaipur, India, Conf. proceedings to appear in Pramana.

[29] S. V. S. Sastry, D. Dutta and D. K. Srivastava, DAE Nuclear Physics Symposium, held at SINP, Calcutta, Dec. 26-30, India, contributed papers, **44B** 288 (2001).

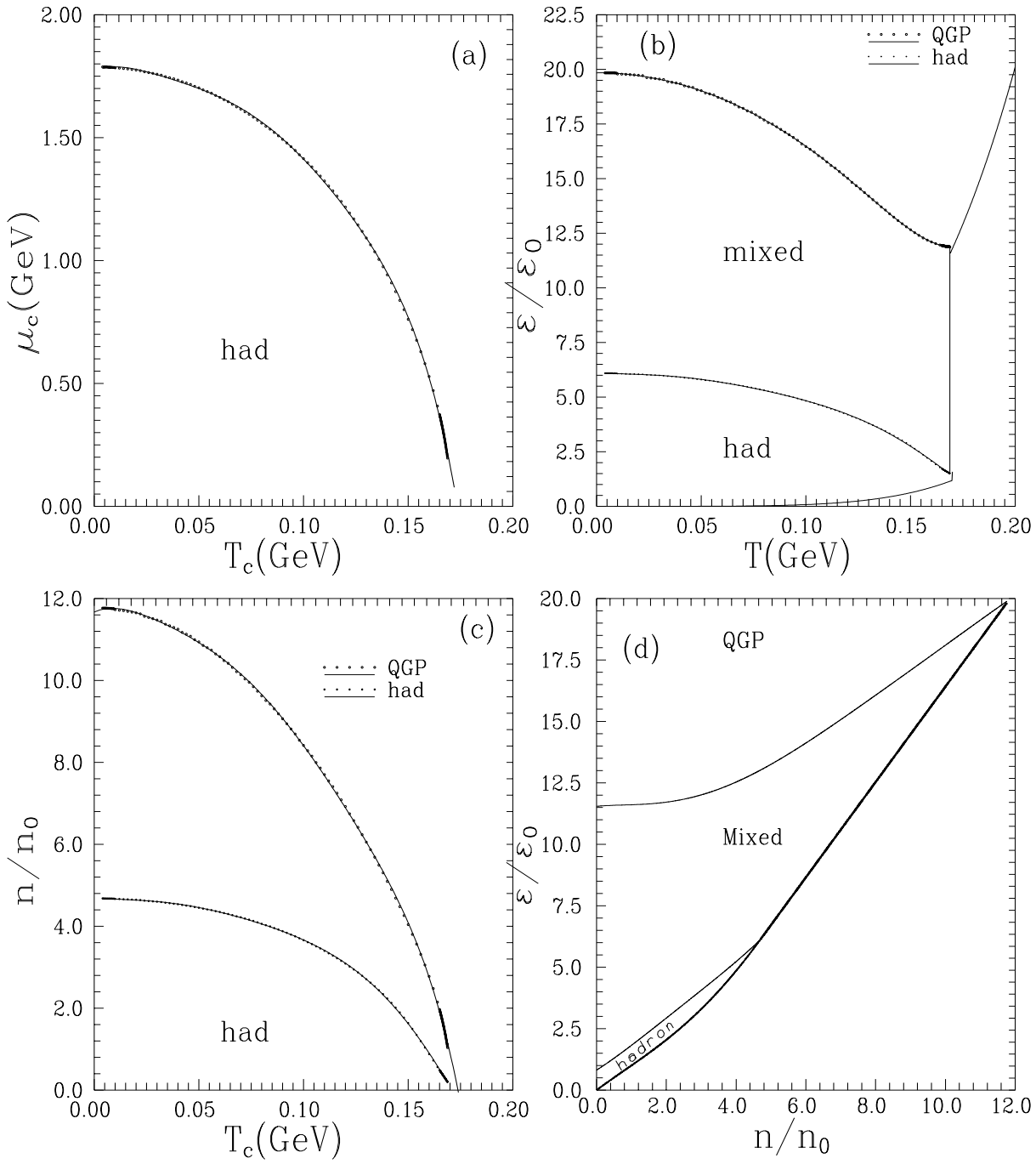

Figure 1: The phase diagram for QGP, Mixed and hadron phases. The phase boundary is obtained from Gibbs conditions.

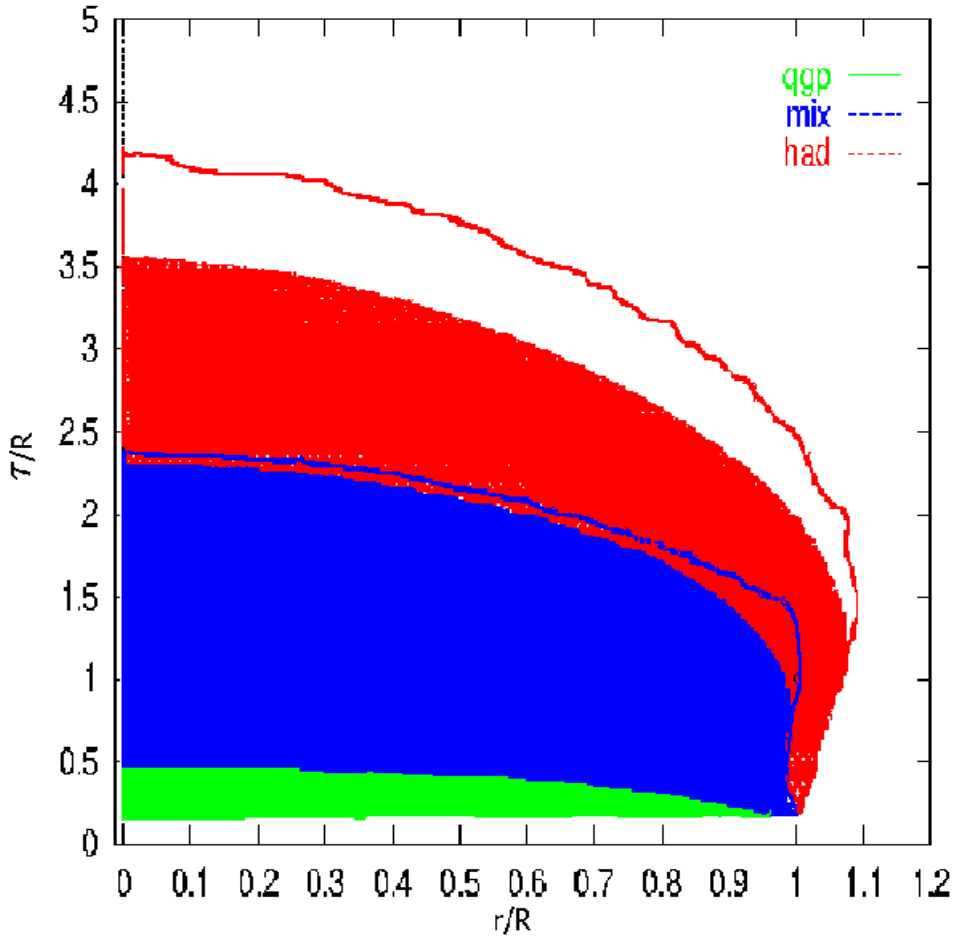

Figure 2: The space-time expansion of the QGP for SPS case. The figure is for finite baryon density, and the corresponding colored solid curves represent the extent of that phase for zero baryon density case.

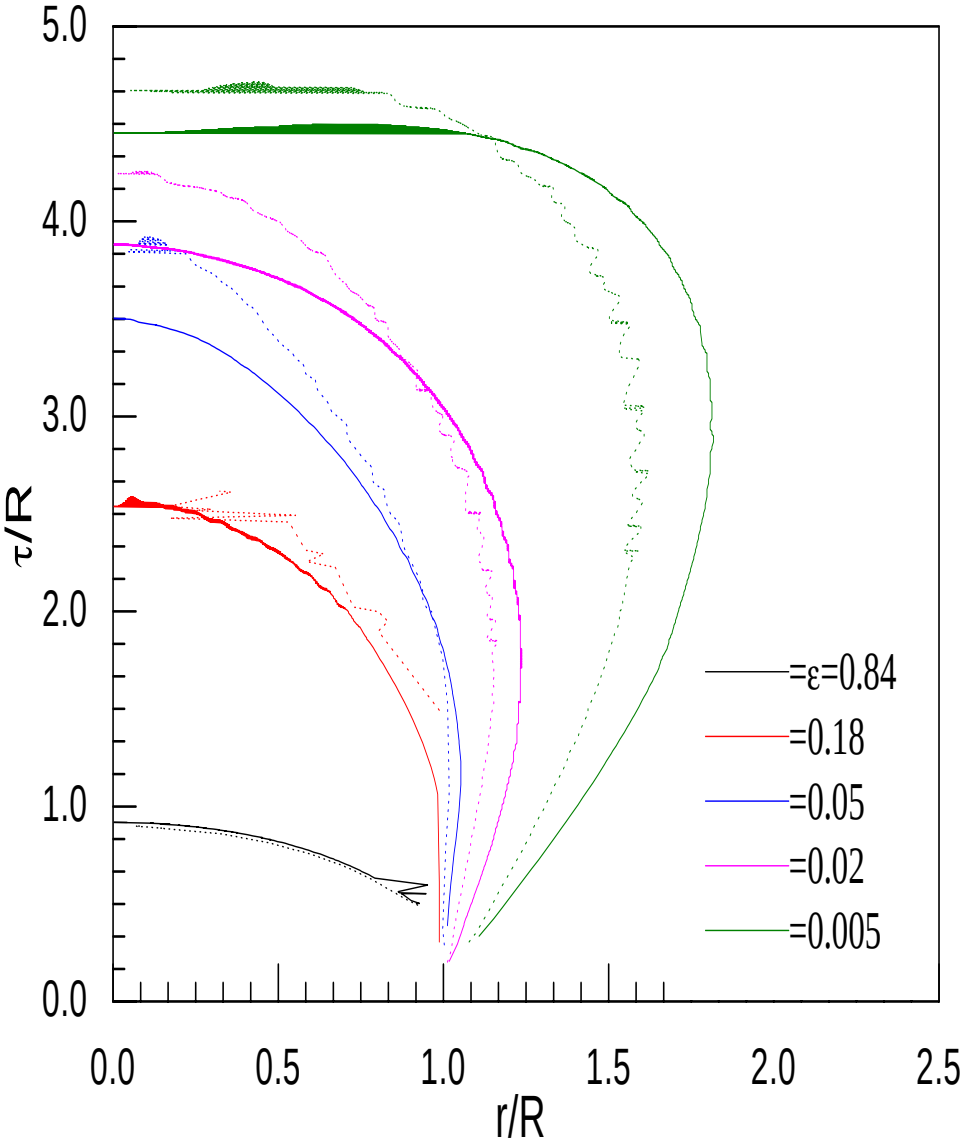

Figure 3: constant energy contours for the SPS energy. The solid curves are with density effects, and the dashed curves are for zero density case.

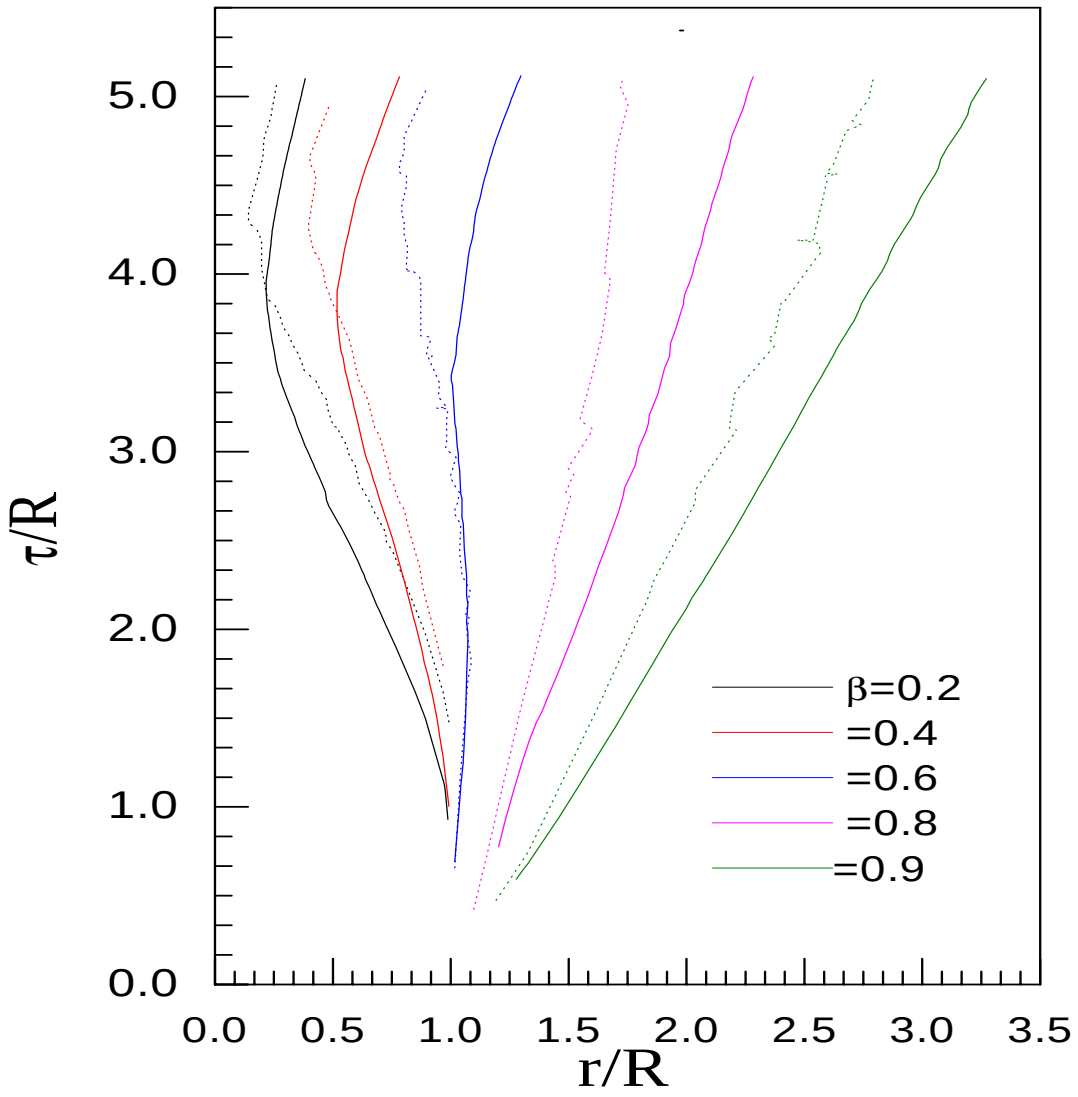

Figure 4: constant velocity contours for the SPS energy. The solid curves are with density effects, and the dashed curves are for zero density case.

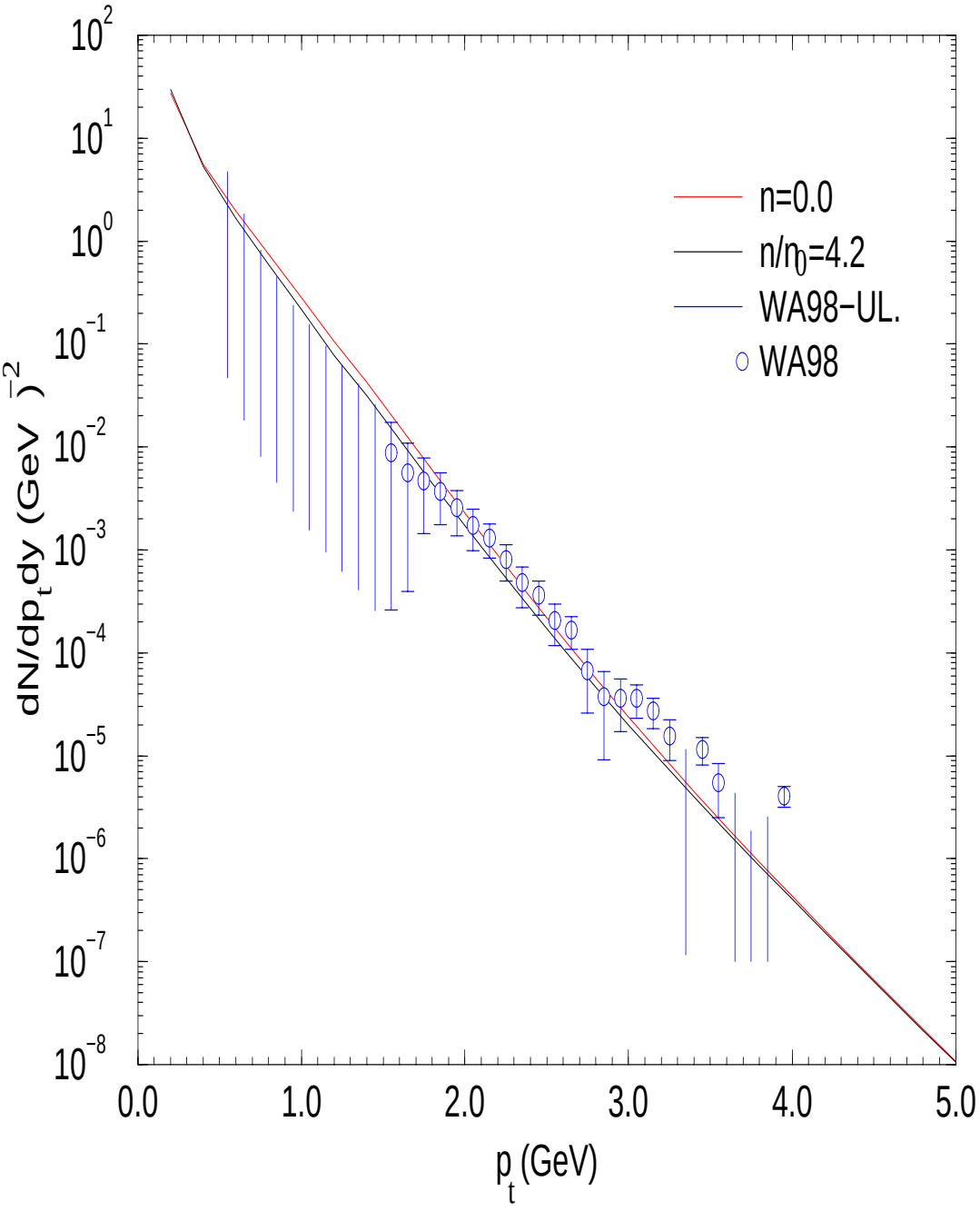

Figure 5: The total space time integrated photon transverse momentum distributions for the SPS case with and without baryon density.

x

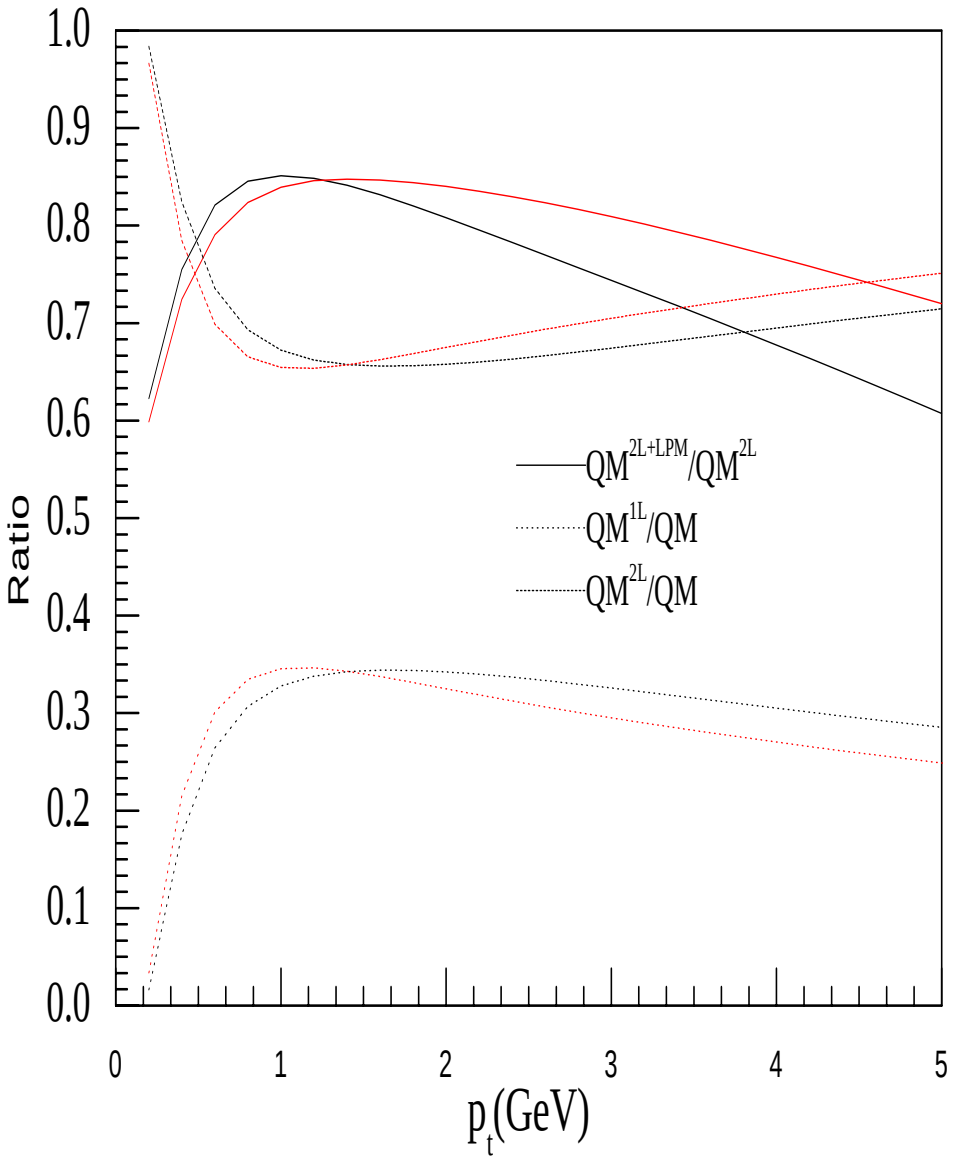

Figure 6: The suppression factor, for the two loop processes consisting bremsstrahlung and aws processes from QGP phase, arising from LPM effects. The LPM effect is shown by solid curves, the dotted curve shows the relative one loop contributions in total quark matter for the photon yields and similarly the dashes are for the relative two loop contribution.